



## Marine CSEM methods for 3D hydrocarbon field mapping and monitoring

Jurgen J. Zach ([jjz@emgs.com](mailto:jjz@emgs.com)), Michael A. Frenkel ([maf@emgs.com](mailto:maf@emgs.com)), Anne-Marit Ostvedt-Ghazi ([amghazi@emgs.com](mailto:amghazi@emgs.com)), Patricia de Lugao ([patricia.lugao@strataimage.com](mailto:patricia.lugao@strataimage.com)), David Ridyard ([dr@emgs.com](mailto:dr@emgs.com)): EMGS Americas

Copyright 2009, SBGf - Sociedade Brasileira de Geofísica

This paper was prepared for presentation during the 11<sup>th</sup> International Congress of the Brazilian Geophysical Society held in Salvador, Brazil, August 24-28, 2009.

Contents of this paper were reviewed by the Technical Committee of the 11<sup>th</sup> International Congress of the Brazilian Geophysical Society and do not necessarily represent any position of the SBGf, its officers or members. Electronic reproduction or storage of any part of this paper for commercial purposes without the written consent of the Brazilian Geophysical Society is prohibited.

### Abstract

The marine Controlled-Source Electromagnetic (CSEM) method has become a well-established geophysical tool for 3D imaging of multiple resistive bodies. While traditionally considered an exploration tool, improved data quality and advanced processing methods put mapping the resistivity distribution within the field in reach, which we demonstrate using a recent survey example from the Norwegian Sea. The survey was acquired in a full 3D grid with state-of-the-art data acquisition standard, which permits advanced processing of full azimuthal data with both consistent phase and magnitude of the horizontal electric and magnetic fields. A resistivity image of a field was obtained using 3D inversion with fast turn-around time, based on approximate Hessian-based optimization and finite-difference time-domain modeling. Particularly in conjunction with 3D- and 4D-seismic technology defining the structural container, marine CSEM can add a complementary image of the bulk distribution of resistors. Using real data and supported by modeling, we assess the capability of CSEM technology for time-lapse monitoring, including the dominant sources of non-repeatability.

### Introduction

Commercial hydrocarbon exploration using marine controlled-source electromagnetic (CSEM) methods using ocean bottom receivers and a ship-towed dipole have been used since 2002 (Eidesmo et al., 2002) and have experienced rapid growth in technology and market penetration. The principal detection mechanism is the relative enhancement of the transverse magnetic component of the received electromagnetic signal by resistors buried in the subsurface. These resistors can be either hydrocarbon deposits or other resistive bodies. The source is comprised by a horizontal bipole, which emits a periodic signal consisting of a number of discrete frequencies which form the basis for survey design, processing and data inversion.

A vast improvement in data quality over the past years was driven by advances in hardware and operations, permitting the acquisition of well-defined and repeatable grids of seabed receivers with complex towing patterns including the acquisition of wide-azimuth data. Together with advances in inversion and integrating CSEM data into global geophysical interpretations, marine CSEM

have become an established method for 3D imaging of complex geological settings, either as a standalone method or in conjunction with other geophysical probes, such as seismic (Norman et al., 2008) or MT (Commer et al., 2008). Particularly, Buonora et al., 2008, have demonstrated the need to integrate marine CSEM into the global exploration workflow. Recent notable case studies include Carrazone et al., 2008, Price et al., 2008 and Plessix, van der Sman, 2008.

While depth migration of CSEM data has been demonstrated in simple cases (Mittet et al., 2005), all commercially viable solutions for 3D imaging of the subsurface rely on a gradient-based, iterative inversion approach in which the full set of Maxwell's equations is solved on a finite grid during each iteration step. The model change after each step is determined from the gradient  $g = \partial \epsilon / \partial \sigma_i$  of a misfit functional  $\epsilon$  with respect to the conductivities in the present discretized model  $\sigma_i$ . The most common representation of the misfit is the L2-norm:

$$\epsilon = \sum_{s,r,\omega,F} (\text{Weight})(\bar{x}_r | \bar{x}_s; \omega) \left| \Delta F_i(\bar{x}_r | \bar{x}_s; \omega) \right|^2, \text{ where}$$

the difference field  $\Delta F_i$  ( $F=E$  and/or  $H$ ) includes both magnitude and phase. This constitutes a full-waveform inversion, which is more robust in CSEM compared to the seismic case on account of the lower resolution due to the diffusive nature of the wave-field compared to the latter. Among the notable recent publications on inversion are for example Commer et al., 2008 (joint CSEM and MT inversion), Jing et al., 2008, who show the importance of including anisotropy in cases where it is relevant, and Gribenko and Zhdanov, 2007. See also Zach et al., 2008-1, which describes the methodology the inversion presented here is based on, as well as references therein.

There is considerable added value in joint interpretation of CSEM and seismic surveys. The complementary relation between the methods has two major aspects:

- (1) Seismic techniques are sensitive to structural boundaries, whereas CSEM anomalies depend on the existence of a sufficient contrast in transverse resistance  $R_t = (\Delta \rho)(\Delta z)$  and are thus sensitive to the bulk volume of a resistor (hydrocarbons or other); it is important to note that  $\Delta z$  can be considerably smaller than the inherent resolution of the method.
- (2) CSEM responds to resistivity, which tends to be sensitive to changes between high to intermediate hydrocarbon saturation, as opposed to seismic attributes such as the p-wave velocity, which is flat in the same saturation range. Conversely, CSEM has little sensitivity to fizz gas compared to 3D seismic techniques. See figure 1, which shows the Gassman p-wave velocity compared to the Archie resistivity as a function of brine saturation.

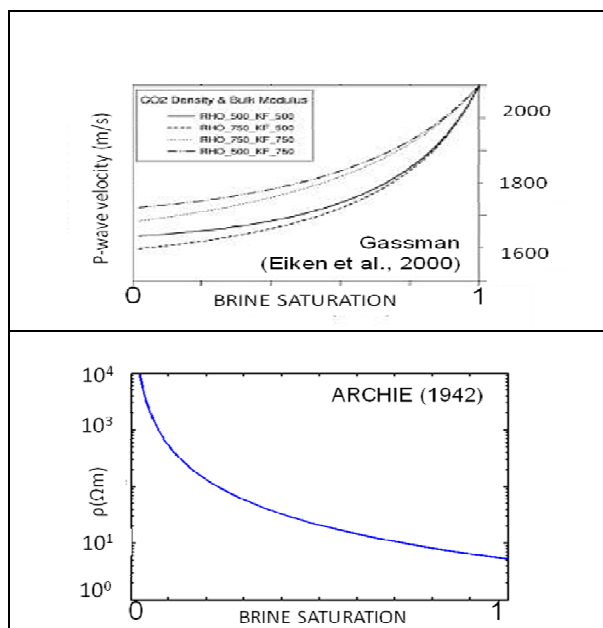


Figure 1: TOP: Seismic p-wave velocity versus the brine saturation (Eiken et al., 2000). BOTTOM: Resistivity versus brine saturation following Archie (1942).

While joint inversion in the narrow sense is of considerable academic interest (e.g., Hoversten et al., 2006), present-day applications focus either on joint interpretation of 3D seismic images and resistivity cubes from 3D-CSEM inversion, or on using seismic constraints to constrain CSEM-inversion. In the present case study, a dense 3D CSEM grid acquired over an area with high-quality 3D seismic data is inverted and discussed. The next logical step beyond 3D-CSEM surveys are time-lapse-, or 4D-CSEM surveys, and have the greatest potential when jointly acquired with time-lapse seismic data. At this point, published time-lapse CSEM surveys are at the stage of detailed survey planning (e.g., Norman et al., 2008, Lien and Mannseth, 2008). In the present contribution, we will evaluate the time-lapse capability of the acquisition mode at the time of publication, and discuss the first two among the following possible sources of non-repeatability:

- (1) Source navigation and waveform,
- (2) Ocean bottom receiver position and orientation,
- (3) Cultural changes between repeat acquisitions (e.g., additional subsea installations).

#### Method 1: Data Acquisition and Conditioning

##### Source-receiver synchronization

Data acquired in a marine CSEM survey consist of time-series data acquired by ocean bottom receivers, which are arranged in grids or lines. Horizontal electric and magnetic fields (4-component), and optional vertical fields, are recorded every 20ms, as a horizontal bipole is towed <100m above the seafloor, see figure 2. Since the receivers operate autonomously between drop and retrieval, their clocks have to be synchronized to the source, which is accurate to better than 10ms over several days. In order to achieve this accuracy, a temperature-dependent correction is applied to the clock calibration. For a typical 0.25 Hz- mode, this is equivalent

to a phase error between source and receiver of better than 1 degree. This implies controlled amplitude and phase throughout receiver grids outlined in figure 3, which is essential to achieve depth sensitivity in inversion.

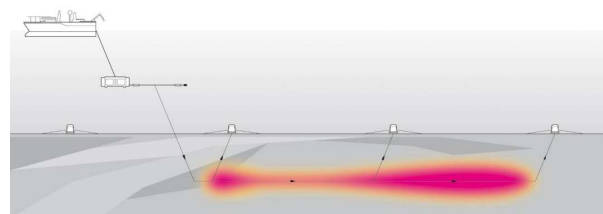


Figure 2: Marine CSEM acquisition mode: a horizontal bipole (~300m), which is towed ~30m above the seafloor emits a periodic current pulse with a peak of up to a few thousand Amperes and a frequency spectrum in the range 0.01-15Hz. Data are comprised by 4- or 6-component electric and magnetic fields recorded at seabed stations arranged in grids with any complexity.

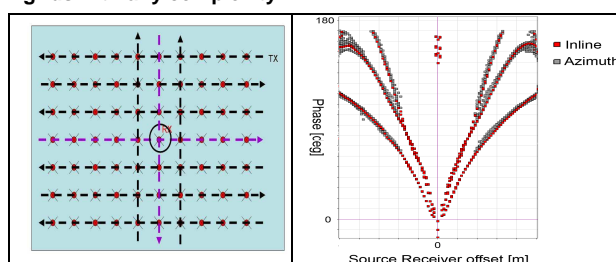


Figure 3: Left: typical grid of receivers with data being recorded for each receiver for both inline (purple) and azimuth (black) lines. Right: Full phase control is demonstrated by plotting the phase one receiver and the 0.25 Hz- and 0.75 Hz-modes for inline and azimuthal data; example from the Norwegian Sea, 2008.

Source navigation data are measured including position and orientation of the source, using a suite of acoustic and echo-sounder sensors on the vessel and the source. However, source navigation accuracy depends on water depth, but is generally given to within ~meters in the horizontal position, ~10 cm in vertical altitude above the seafloor and less than 1 degree for the source dipole orientation. Navigation data are recorded every 10 seconds, and an interpolation method is used to assign a source position to each electric field measurement.

##### Data conditioning for advanced processing

The data conditioning follows the approach outlined in Zach et al., 2008-2, see figure 4. Data are converted into the frequency domain in a demodulation step which employs a short-time Fourier transform over a period approximately equivalent to towing the source over one source length. Data are rotated into the towline, such that the Ex-component points along the towline. The receiver angle is determined with a proprietary data-driven method similar to the one described in Mittet et al., 2007. A cost-efficient direct measurement method of the receiver rotation is under development. It should be stated that no subsequent timing/phase corrections are necessary at the state of the art.

For advanced processing such as inversion, a proper estimation of the data uncertainty is crucial to determine the data weights. Since the noise spectrum in the marine CSEM- frequency range is relatively flat, the noise pertaining to each source frequency can be determined by averaging over a frequency range in the spectral

neighborhood of the main mode (see Zach et al., 2008-2 for details). Data and accordant noise for a recent deep-water acquisition are shown in figure 5.

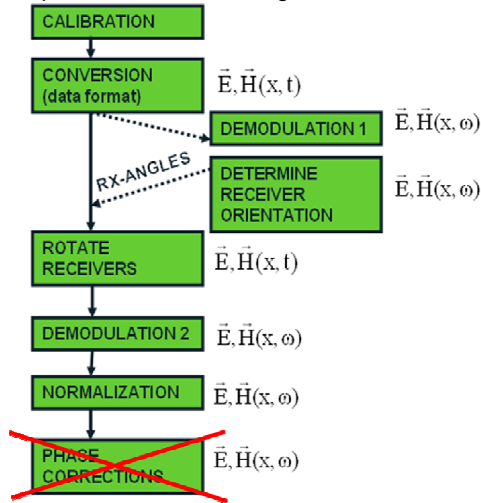


Figure 4: Main steps in preprocessing workflow for frequency-domain 3D inversion of marine CSEM data.

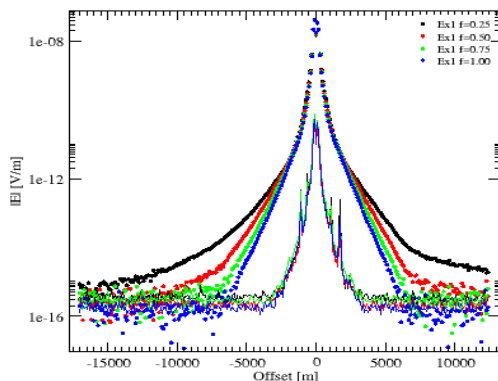


Figure 5: Magnitude-versus-offset curve for a receiver in a recent deep-water acquisition. The scatter curves show the inline (i.e., in the same direction of the source bipole) component of the electric magnitude for a composite input pulse with four major frequencies, and the line curves the noise.

*Starting model generation*

Due to the sensitivity of a gradient-based inversion scheme, the construction of a starting model which captures the main background trends of the subsurface is essential. Towards that, suitable individual receivers are inverted using a simulated annealing- based plane-layer inversion (Roth and Zach, 2007), and the resulting pseudo-well profiles extrapolated below the bathymetry, which is typically known from prior seismic surveys. In case well logs are available which can be extrapolated to the survey area in a meaningful way and for which anisotropy information exists, these are included in the starting model building.

**Method 2: 3D INVERSION OF MARINE CSEM DATA**

*Inversion loop*

The 3D inversion methodology applied here is based on Zach et al., 2008-1, see the inversion loop in figure 6. The gradient calculation is based on the first Born-scattering

assumption of the relationship between model- and field-perturbation (Støren et al., 2008). A fast finite-difference time-domain solver based on Maaø, 2007 was used to generate synthetic data. The optimization is based on a quasi-Newton update using the known gradient and an approximate calculation of the inverse Hessian matrix.

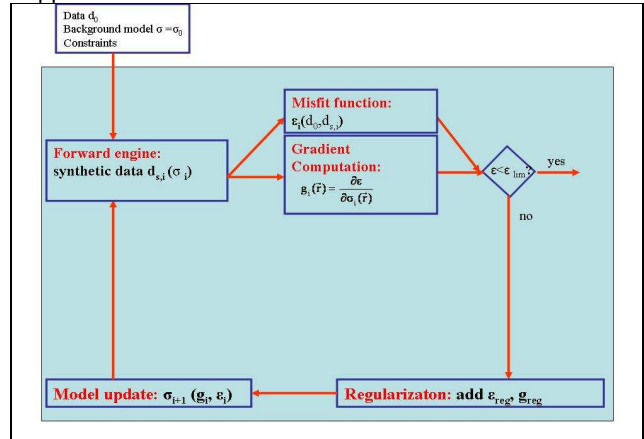


Figure 6: Iterative loop for gradient-based inversion, consisting of a forward Maxwell solver, misfit function and gradient calculation, a regularization step and an optimization step.

The model update in figure 6 consists of a quasi-Newton update step:

$$\sigma - \sigma_0 = -v_0 [\nabla^2 \epsilon(\sigma_0)]^{-1} \nabla \epsilon(\sigma_0),$$

where  $v_0$  is a scalar  $< 1$ , the gradient of the misfit functional with respect to a model change is  $g = [\nabla \epsilon] = 0$ ,

and the inverse Hessian matrix  $[\nabla^2 \epsilon]^{-1}$  is approximated using an outer product formulation of the vectors of an integer number  $m$  of past iterations' update steps and gradient changes (Byrd et al., 1995).

**Example from offshore Norway**

A 3D CSEM grid survey with 1.25 km grid spacing, consisting of 54 receivers, was acquired in the Norwegian North Sea in March 2008. The source waveform was mainly a triple peak with the modes 0.25, 0.75 and 1.25 Hz, with approximately equal amplitude on all of them. The target is the Troll oil province, which is shown in figure 7 at the horizontal coordinate  $\sim 523000$ , a few km west of the Troll West gas field, which is a well-known CSEM calibration target. To improve the quality of the data-driven estimate of the receiver rotation angle, the source was towed over each receiver at least once. Figure 8 shows a CMP map for two representative attributes, which already map both the Troll West gas field and the Troll oil province clearly. The level of detailed delineation in the data alone is particularly encouraging, as the latter field constitutes a much more challenging CSEM target than the former.

In the best 3D inversion result of the dataset, only three dominant modes of the electric field were used due to better noise suppression compared to the magnetic field. Due to the pipeline around 1km west of the survey grid acting as a secondary source, the westernmost towline was discarded, so that a total of 45 receivers were inverted. The starting model used was based on measured bathymetry and plane-layer inversion of a

reference receiver. An image of the final resistivity cube is shown in figure 9, which confirms the strong anomaly due to the gas field, the known geology of the area and an outline of the resistive response within the boundaries of the seismic prospect of the Troll oil field. In general, within the resolution of the CSEM method, proven well logs throughout the area are confirmed. Most importantly, the resistivity distribution within the reservoir is visible, for example the gas cap on top of the oil reservoir.

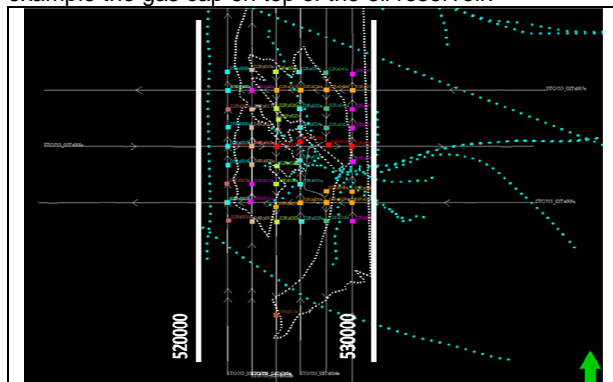


Figure 7: Map over survey area: the 3D grid is represented by colored squares, whereas existing pipelines and prospect outlines are outlined by blue and white dashed lines, respectively.

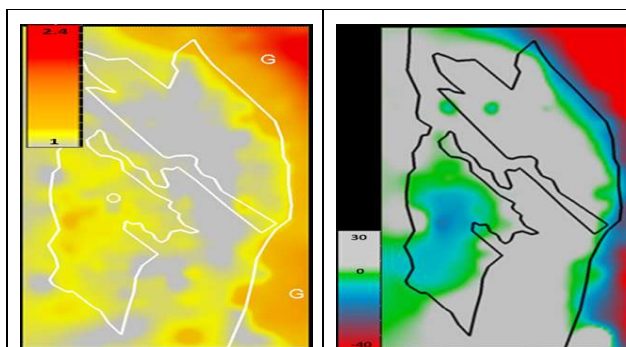


Figure 8: Selected CMP-attribute maps for electric data normalized to a reference receiver in a 5000+/-250 m offset bin. Left: 0.25 Hz, normalized magnitude. Right: 1.25 Hz, phase difference. Both the Troll oil province and the Troll West gas field are clearly marked by data anomalies.

**Conclusion: 3D-CSEM**

We have presented a robust inversion-based 3D interpretation approach which is, together with constraints from seismic and/or well data, able to quantitatively map resistivity within a reservoir. The time for one inversion to converge to the accuracy of the marine CSEM method (<5% in magnitude, <5 degrees in phase) is typically about one week.

**The next step: 4D-CSEM**

*Sources of non-repeatability*

In past surveys, the greatest acquisition uncertainty related to the receiver orientation, which introduced a systematic error of up 3-5 degrees from the receiver azimuthal rotation angle and receiver/electrode tilt. However, new proprietary data-driven algorithms as well as direct measurements of the orientation will rapidly reduce this uncertainty. Moreover, placing seabed

monuments on desired receiver locations is both technically and commercially feasible in a time-lapse monitoring scenario. Hence, future sources of non-repeatability will be dominated by the source navigation. Table 1 lists the present versus future contributions of the most relevant source parameters to the time-lapse error.

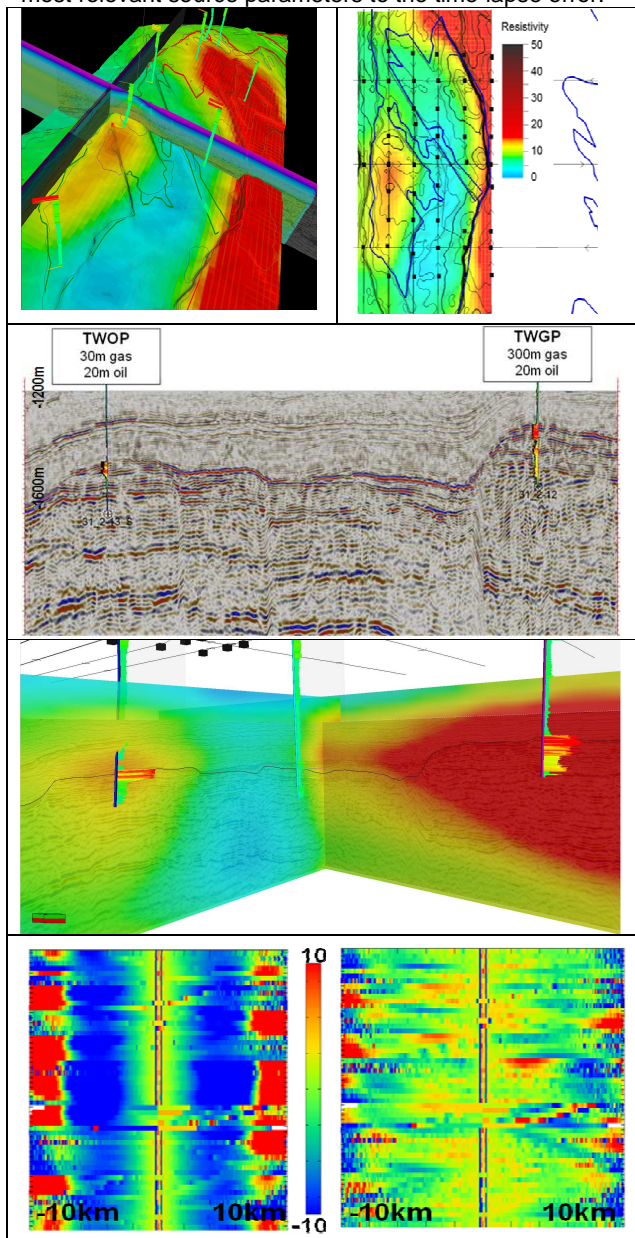


Figure 9: Final inversion result for 3D inversion of electric data including both inline and azimuthal fields from the grid shown in figure 7 over the Troll oil province. First panel: Resistivity in inversion cube draped onto prospect level; second panel: seismic section through two principal wells in both the Troll oil- and Troll West gas province; third panel: panoramic view, comparing true resistivity in well logs with CSEM inversion response; fourth panel: color-coded phase convergence plot for the entire inverted 3D survey (color scale represents phase deviation between real and synthetic data for the starting model (left) and the final model (right)) showing consistency to within 5 degrees throughout the survey.

Parameter	Present-day receiver data error	Mitigate effect on time-lapse with present-day technology	Further mitigation with moderate technology upgrade
<b>Source altitude</b> 	<2% for $\Delta=5\text{m}$	Corrections based on modeling or re-datuming possible; fully implemented in inversion. Aim for survey plan in flat bathymetry.	Improve with better source position information & navigation: ~1-3m accuracy expected.
<b>Source tilt</b> 	<3% for 5 dgr.	Modeling-based correction possible; fully implemented in inversion. Aim for flat bathymetry where possible.	Improve with better source position information & navigation: within 1 dgr. Parallel to seafloor expected.
<b>Source path offset</b> 	<1% for $\Delta<50\text{m}$	Minor problem due to accurate receiver positioning; fully implemented in inversion.	Better receiver positioning, source navigation. Acquisition standards approach 10m.
<b>Source feathering</b> 	1-5% for 10 degrees	Modeling-based correction possible; fully implemented in inversion. Attempt repeating survey in similar ocean current conditions.	Better source navigation, actively steered source.

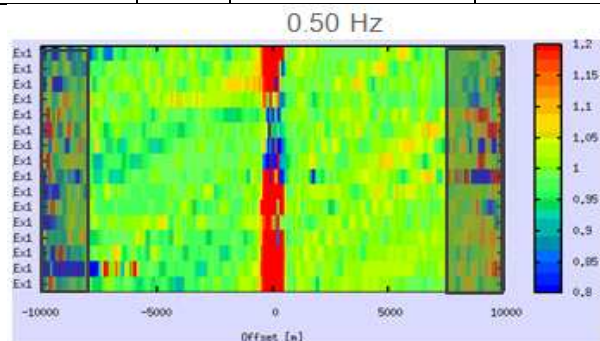


Figure 10: Time-lapse repeatability: relative magnitude versus offset of inline electric data, whereby subsequent tows were normalized against each other.

The cumulative error based on source navigation only from a recent dataset in the Gulf of Mexico, where part of a survey was towed twice over the same receiver drop, is shown in figure 10, where the resulting time-lapse repeatability is within 3-5%.

*Time-lapse feasibility modeling*

One of the key potential 4D-CSEM applications is time-lapse waterflood monitoring in hydrocarbon reservoirs, particularly to distinguish different shapes of the advancing waterfront. Figure 11 shows a numerical experiment with a 10km x 10km reservoir, one fifth of which is flooded from the left. In both cases, the volume of the flood is the same, but the shape is different, representing compartmentalized reservoirs. As time-lapse responses, we consider the measured field after versus before flooding, which are plotted for three receiver lines in figure 12. Only the Eastern electric field component is plotted, and only responses are plotted for which the received signal is at least one order of magnitude above the noise threshold (assumed to be  $10^{-15}\text{V}/\text{Am}^2$ ). The flood causes a 30%-50% anomaly level, whereas different realistic flooding patterns can distinguish each other on a 10% anomaly level. With a 5% repeatability error in time-lapse surveys established with today's marine CSEM technology, we therefore conclude that in large reservoirs, both production and water flood as such, as well as different shapes of water flood can be monitored.

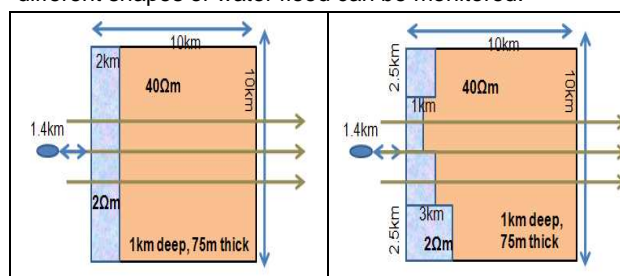


Figure 11: Top view of reservoir model with two different shapes of identical volume water floods. The source bipole is located 6.4km to the left of the reservoir edge, and the received signal is compared along the three olive-green lines shown.

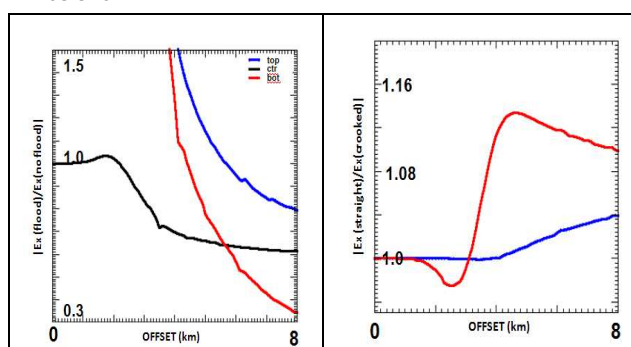


Figure 12: Time-lapse signal for the water flood shown in figure 11. Top: for  $f=0.25\text{ Hz}$ , the Eastern electric field after versus before the flood for the three lines shown in the right panel of figure 11. The anomaly is detectable on a 30%-50% anomaly level. Bottom: the Eastern electric field of the "crooked" flood on the right versus the "straight" flood on the left. The relative difference in the signal between both flood shapes is therefore detectable, if a time-lapse error of ~5% is assumed. Color legend: blue: top line, red: bottom line, black: center line in fig. 11.

Finally, figure 13 shows the relative time-lapse signal of a partial water flood, showing a 20%-anomaly, even if the resistivity only decreases by 50%, also resolvable using state of the art-CSEM surveys. Dedicated time-lapse workflows and inversion algorithms are presently under development.

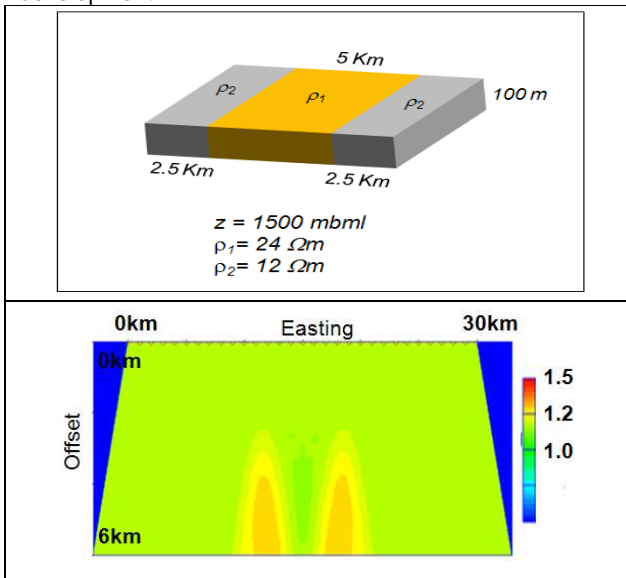


Figure 13: Water flood (grey) in a hydrocarbon reservoir (orange) at 1.5 km below sea level. Top: schematic of the reservoir. Bottom: normalized time-lapse signal of produced versus unproduced reservoir (CMP-line summary plot over CSEM receiver line over center of reservoir).

#### Acknowledgments

We thank StatoilHydro for the right to present the data and results of the 3D acquisition of the Troll oil province, and EMGS for supporting this contribution. Particularly, we thank Jaime Hincapie and Honglin Yuan (EMGS) for their support for geological modeling.

#### References

- Archie, G.E., 1942, The electrical resistivity log as an aid in determining some reservoir characteristics. *Trans. Am. Inst. Mech. Eng.* 146, 54-62.
- Buonora, M.P., Zerilli, A., Labruzzo, T., Rodrigues, L.F., 2008, Advancing Marine Controlled Source Electromagnetics in the Santos Basin, Brazil. *EAGE 2008 Expanded Abstracts, Rome, Italy.*
- Byrd, R.H., Lu, P., Nocedal, J., 1995, A Limited Memory Algorithm for Bound Constrained Optimization. *SIAM Journal on Scientific and Statistical Computing*, 16, 5, 1190-1208.
- Carrazone, J.J., Dickens, T.A., Green, K.E., Jing, C., Wahrmond, L.A., Willen, D.E., Commer, M., Newman, G.A., 2008, Inversion study of a large marine CSEM survey. *SEG 2008 Expanded Abstracts, Las Vegas, NV, USA.*
- Commer, M., Newman, G.A., 2008, Optimal conductivity reconstruction using three-dimensional joint and model-based inversion for controlled-source and magnetotelluric data, *SEG 2008 Expanded Abstracts, Las Vegas, NV, USA.*

- Eidesmo, T., Ellingsrud, S., MacGregor, L.M., Constable, S., Sinha, M.C., Johansen, S., Kong, F.N. and Westerdahl, H., 2002, Sea Bed Logging (SBL), a new method for remote and direct identification of hydrocarbon filled layers in deepwater areas. *First Break*, 20, 144-152.
- Eiken, O., Brevik, I., Arts, R., Lindeberg, E., Fagervik, K., 2000, Seismic monitoring of CO<sub>2</sub> injected into a marine aquifer. *SEG 2000 Expanded Abstracts, Calgary.*
- Gribenko, A., Zhdanov, M., 2007, Rigorous 3D inversion of marine CSEM data based on the integral equation method. *Geophysics*, 72, WA73-WA84.
- Hoversten, G.M., Cassassuce, F., Gasperikova, E., Newman, G.A., Chen, J., Rubin, Y., Hou, Z., Vasco, D., 2006, Direct reservoir parameter estimation using joint inversion of marine seismic AVA and CSEM data, *Geophysics* 71, C1-C13.
- Jing, C., Green, K.E., Willen, D.E., 2008, CSEM inversion: Impact of anisotropy, data coverage, and initial models. *SEG 2008 Expanded Abstracts, Las Vegas, NV, USA.*
- Lien, M., Mannseth, T., 2008, Sensitivity study of marine CSEM data for reservoir production monitoring, *Geophysics* 73, F151.
- Maaø, F. A., 2007, Fast finite-difference time-domain modeling of marine-subsurface electromagnetic problems. *Geophysics*, 72(2), A19-A23.
- Mittet, R., Aakervik, O.M., Jensen, H.R., Ellingsrud, S., Stovas, A., 2007, On the orientation and absolute phase of marine CSEM receivers. *Geophysics* 72, F145-F155.
- Mittet, R., Maaø, A.F., Aakervik, O.M., 2005, A two step approach to depth migration of low-frequency electromagnetic data. 75<sup>th</sup> Annual International Meeting, SEG, Houston, TX, USA, Expanded Abstracts, 522-525.
- Norman, T., Alnes, H., Christensen, O., Zach, J.J., Eiken, O., Tjøland, E., 2008, Planning Time-lapse CSEM-surveys for Joint Seismic-EM Monitoring of Geological Carbon Dioxide Injection. *EAGE Budapest 2008 CO2 Geological Storage Workshop.*
- Plessix, R.-E., van der Sman, P., 2008, Regularized and blocky controlled source electromagnetic inversion. *PIERS 2008, Cambridge, Mass.*
- Price, A., Turpin, P., Erbetta, M., Watts, D., Cairns, G., 2008, 1D, 2D and 3D modeling and inversion of 3D CSEM data offshore West Africa. *SEG 2008 Expanded Abstracts, Las Vegas, NV, USA.*
- Roth, F., Zach, J.J., 2007, Inversion of marine CSEM data using up-down wavefield separation and simulated annealing. *SEG 2007 Expanded Abstracts, San Antonio, TX, USA.*
- Støren, T., Zach, J.J., Maaø, F., 2008, Gradient calculations for 3D inversion of CSEM data using a fast finite-difference time-domain modelling code, *EAGE 2008 Expanded Abstracts, Rome, Italy.*
- Zach, J.J., Bjørke, A.K., Støren, T., Maaø, F., 2008-1, 3D inversion of marine CSEM data using a fast finite-difference time-domain forward code and approximate Hessian-based optimization. *SEG 2008 Expanded Abstracts, Las Vegas, NV, USA.*
- Zach, J.J., Roth, F., Yuan, H., 2008-2, Data preprocessing and starting model preparation for 3D inversion of marine CSEM surveys. *EAGE 2008 Expanded Abstracts, Rome, Italy.*